

Article

Computational Methods in the Drug Delivery of Carbon Nanocarriers onto Several Compounds in Sarraceniaceae Medicinal Plant as Monkeypox Therapy

Fatemeh Mollaamin

Department of Biology, Faculty of Science, Kastamonu University, Kastamonu 37100, Turkey; smollaamin@gmail.com

Abstract: In this article, monkeypox is studied as a zoonotic poxvirus disease which can occur in humans and other animals due to substitution of the amino acid serine with methionine. We investigate the (+)-catechin, betulinic acid, ursolic acid, quercetin-3-O-galactoside, luteolin-7-O-glucoside, and myricetin in *Sarracenia purpurea* drugs from Sarraceniaceae family for treating monkeypox disease. This is performed via adsorption onto the surface of (6,6) armchair single-walled carbon nanotube (SWCNT) at the B3LYP/6-311+G (2d,p) level of theory in a water medium as the drug delivery method at 300 K. *Sarracenia purpurea* has attracted much attention for use in the clinical treatment of monkeypox disease due to the adsorption of its effective compounds of (+)-catechin, betulinic acid, ursolic acid, quercetin-3-O-galactoside, luteolin-7-O-glucoside, and myricetin onto the surface of (6,6) armchair SWCNT, a process which introduces an efficient drug delivery system though NMR, IR and UV-VIS data analysis to the optimized structure. In addition to the lowering of the energy gap ($\Delta E = E_{LUMO} - E_{HOMO}$), HOMO–LUMO energy has illustrated the charge transfer interactions taking place within (+)-catechin, betulinic acid, ursolic acid, quercetin-3-O-galactoside, luteolin-7-O-glucoside, and myricetin. The atomic charges have provided the proper perception of molecular theory and the energies of fundamental molecular orbitals.

Keywords: monkeypox disease; *Sarracenia purpurea*; (+)-catechin; betulinic acid; ursolic acid; quercetin-3-O-galactoside; luteolin-7-O-glucoside; myricetin (6,6) armchair CNT



Citation: Mollaamin, F. Computational Methods in the Drug Delivery of Carbon Nanocarriers onto Several Compounds in Sarraceniaceae Medicinal Plant as Monkeypox Therapy. *Computation* **2023**, *11*, 84. <https://doi.org/10.3390/computation11040084>

Academic Editors: Amal Khalifa and Simeone Marino

Received: 15 February 2023

Revised: 29 March 2023

Accepted: 17 April 2023

Published: 20 April 2023



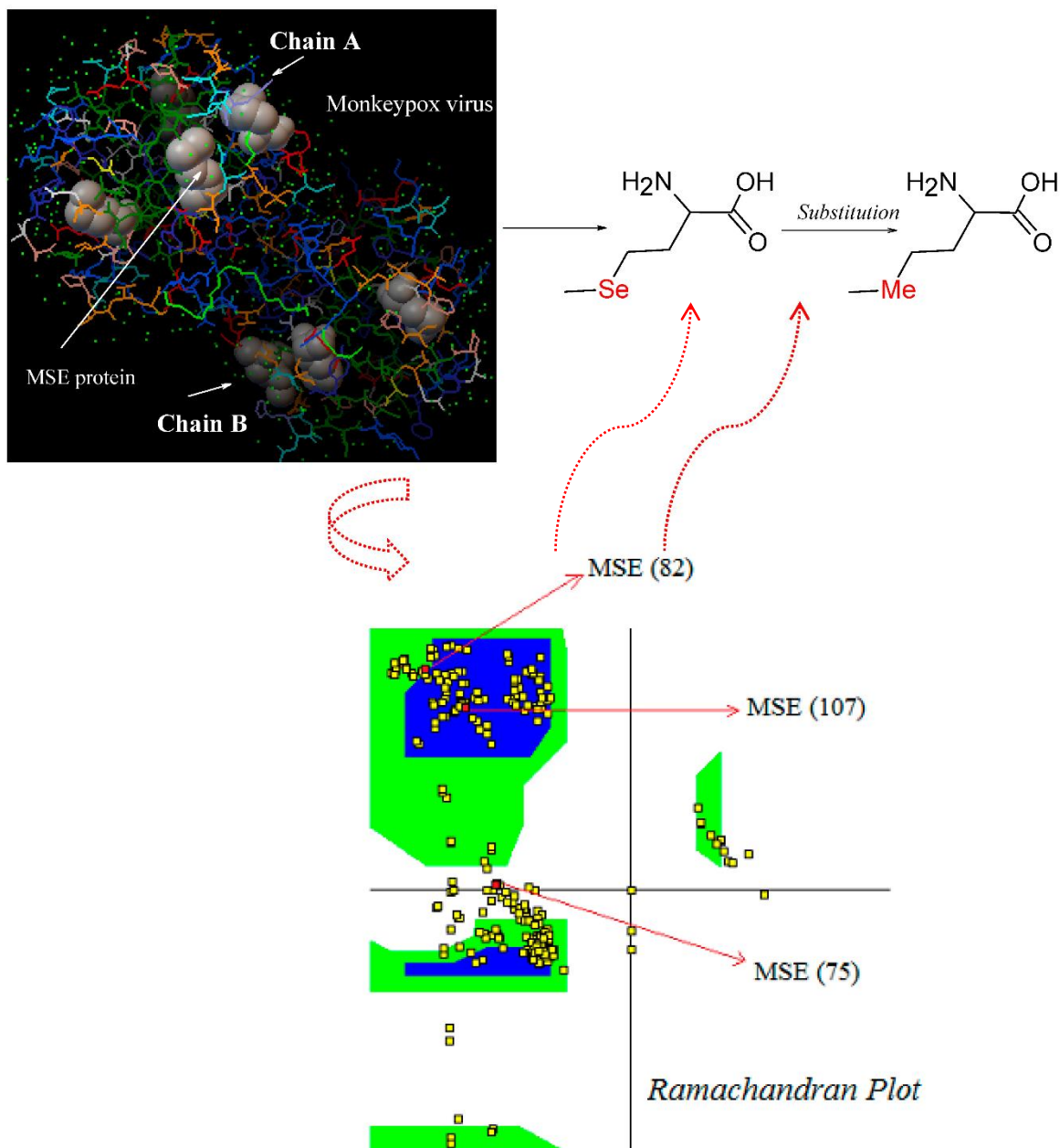
Copyright: © 2023 by the author. Licensee MDPI, Basel, Switzerland. This article is an open access article distributed under the terms and conditions of the Creative Commons Attribution (CC BY) license (<https://creativecommons.org/licenses/by/4.0/>).

1. Introduction

The Monkeypox virus can cause infectious diseases in the human body and sometimes in other animals. The virus causes the symptoms of muscle ache, swollen lymph nodes, and pimples accompanying a fever that produces smallpox, which peels little by little until disappearing [1]. Over a period of several weeks, the symptoms become weaker, but sometimes are strong, especially in people with vulnerable health [1–3]. This virus causes a type of chickenpox orthopoxvirus and may be distributed due to bush meat, animal scrapes or stings, bodily liquids, contaminated ingredients or sick people through the air or droplets [4,5]. In 2014, Minasov and co-workers discovered the crystal structure of A42R profilin-like protein from the Monkeypox virus using X-ray diffraction [6]. It was seen that the amino acid of serine in the target of L-PEPTIDE LINKING, which has the formula $C_5H_{11}NO_2Se$ from the A42R profilin-like protein, was substituted with methionine, a fact which has been shown by MSE protein MSE (1), MSE (75), MSE (82), and MSE (107) in two chains of A and B with (Scheme 1).

Although there is no cure for the monkeypox disease, the smallpox vaccine could be efficient in preventing putrefaction in close connections and in reducing the hardness of the disease. During spread, some antiviral medications and chemical drugs might be applied, as might the smallpox vaccine [7,8]. Moreover, medicinal plants and herbal practices have been used to treat viral diseases for decades. Although rarely studied, these medicinal plants could serve as strong foundations for novel antiviral drugs with applications versus

rising and increasing viral diseases such as monkeypox, smallpox, yellow fever, Lassa fever, meningitis, and COVID-19.



Scheme 1. 3D structure of Monkeypox virus with two chains of A and B, MSE protein, Ramachandran Plot and substitution of serine with methionine in the target.

A research work by Arndt and his co-workers demonstrated the in vitro characterization of *Sarracenia purpurea* to be the first effective inhibitor of poxvirus replication at the level of early viral transcription. With the renewed threat of poxvirus-related infections, their results showed that *Sarracenia purpurea* might act as another defensive measure against orthopoxvirus infections [9].

Recently, scientists indicated the potential of scarcely investigated and uninvestigated natural drugs when applied to curing COVID-19, yellow fever, smallpox, monkeypox, hepatitis, poliomyelitis, Lassa fever, and meningitis [10]. Understanding disease ecology could help to preventing transmission and curb its spread. The established treatment protocols along with the development of new antiviral agents and vaccines could play a pivotal role in controlling transmission.

Abubakar and his research group aimed to document the herbal practices and medicinal plants used to treat monkeypox and other emerging and re-emerging viral diseases [11].

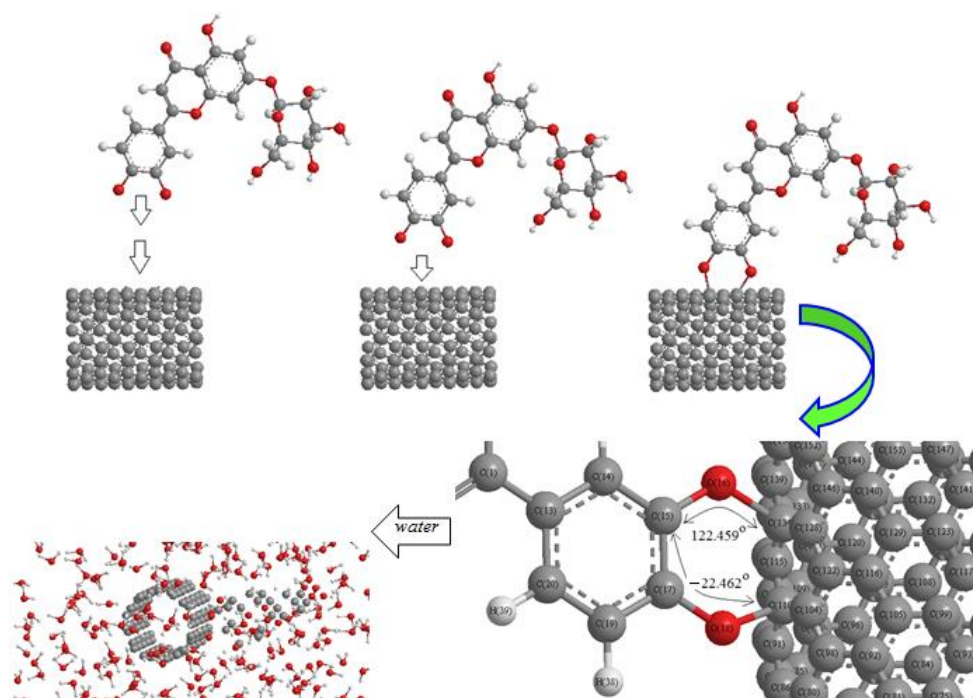
In this work, we have investigated the physico-chemical characteristics of effective compounds of the medicinal plant, *Sarracenia purpurea*, including (+)-catechin, betulinic acid, ursolic acid, quercetin-3-O-galactoside, luteolin-7-O-glucoside, and myricetin. This plant is employed to treat smallpox, cowpox and monkeypox.

It has been investigated that *Sarracenia purpurea* can be an inhibitor of the orthopoxvirus protein, a fact which is exhibited by its being the cure for human smallpox disease. The impact of *Sarracenia purpurea* might decrease in patients with impaired immune systems [12,13].

There is a focus on enhancing the bioavailability and duration of action of a drug in order to modify its therapeutic effect. Drug delivery technique is able to change a drug's pharmacokinetics and specificity by formulating it with various ingredients, drug carriers, and pieces of medical equipment [14–18]. Nanomedicine in drug delivery can achieve the improved delivery of water insoluble drugs, the delivery of large macromolecule drugs to intracellular sites of action, and the codelivery of two or more drugs or therapeutic agents for use in combination remedy [19–21].

Nanotubes, with their intrinsic properties, have been considered potential candidates for drug delivery carriers. The capped ends of nanotubes may be opened up by oxidation, allowing for the insertion of molecules of interest inside the nanotubes. Carbon nanotubes (CNTs) can easily penetrate cells, delivering drugs directly to the cytoplasm or nucleus. Nanotubes conform to a perpendicular position to the cell membrane during uptake, perforating and diffusing through the lipid bilayer to enter the cytoplasm. Functionalized CNTs are easily internalized by cells through passive and endocytosis-independent mechanisms [22–27].

In this research, we have focused on (+)-catechin, betulinic acid, ursolic acid, quercetin-3-O-galactoside, luteolin-7-O-glucoside, and myricetin, adsorbed onto the surface of (6,6) armchair SWCNT in a water medium for preventing the activity of the monkeypox virus (Scheme 2).



Scheme 2. Mechanism of adsorption of luteolin-7-O-glucoside onto the surface of (6,6) armchair SWCNT in a water medium at 300 K.

The structure of (+)-catechin, betulinic acid, ursolic acid, quercetin-3-O-galactoside, luteolin-7-O-glucoside, and myricetin in the *Sarracenia purpurea* medicinal plant (a car-

nivorous plant in the Sarraceniaceae family) has been investigated in this study as a relatively stable drug for adsorption onto the surface of (6,6) armchair SWCNT through the drug delivery method (Scheme 2). Thus, a series of quantum theoretical approaches, including DFT methods, has been used in order to find the optimized coordination of (+)-catechin, betulinic acid, ursolic acid, quercetin-3-O-galactoside, luteolin-7-O-glucoside, and myricetin, adsorbed onto (6,6) armchair SWCNT by using Gaussian 16 revision C.01 program (Scheme 2) [28]. The adsorption of these compounds onto (6,6) armchair SWCNT has indicated the nature of chemisorption for the bond distance of O–C of about 1.5 Å, with the equilibrium electron diffusion of effective compounds of *Sarracenia purpurea* (adsorbate) and single-walled carbon nanotube (adsorbent) (Scheme 2).

2. Theoretical Frameworks and Computational Methods

The geometric optimization of the compounds in this paper has been performed via the framework of DFT using the three-parameter Becke's exchange [29] and Lee–Yang–Parr's correlation non-local functional [30], usually known as the B3LYP method and basis set of 6-311+G(2d,p). The density functional theory (DFT) is one of the most employed approximations of Hohenberg, Kohn and Sham and allows the theoretical study of material properties [31]. Density functional theory (DFT) represents an advantageous methodology for estimating chemical systems, and discovering its similarities and differences to other computational employed methodologies is of importance [32,33].

Therefore, the electronic structure of adsorbed (6,6) armchair CNT by (+)-catechin, betulinic acid, ursolic acid, quercetin-3-O-galactoside, luteolin-7-O-glucoside, and myricetin in the *Sarracenia purpurea* medicinal plant has been illustrated for use measuring physico-chemical properties (Scheme 2).

In this work, the Onsager model has been used. This was developed by Frisch, Wong and Wiberg and utilizes spherical cavities. Even though this implies a less accurate description of the solute–solvent interface, this approximation simplifies the evaluation of energy formatives in geometry optimizations and frequency analysis. Moreover, Cramer and Truhlar improved this model at the dipole level [34–38]. In fact, a cavity must have a physical sense, such as in the Onsager model, and a mathematical ability, as often demonstrated in other descriptions of solvent impacts [39]. On the other hand, the cavity has to keep out the solvent, including its frontiers, as the largest probability part of the solute charge distribution [39–43].

Basically, a group of quantum theoretical methods has been performed to explore some physical and chemical properties from optimized structure of (+)-catechin, betulinic acid, ursolic acid, quercetin-3-O-galactoside, luteolin-7-O-glucoside, and myricetin in *Sarracenia purpurea* medicinal plant, adsorbed onto the surface of (6,6) armchair CNT. This includes charge distribution, thermodynamic calculations and nuclear magnetic resonance analysis due to designing a drug delivery model using Gaussian 16 revision C.01 program [28]. Moreover, the gauge-including atomic orbitals (GIAO) have been adopted to solve the gauge problem in the calculation of nuclear magnetic shielding for [(+)-catechin, betulinic acid, ursolic acid, quercetin-3-O-galactoside, luteolin-7-O-glucoside, and myricetin in *Sarracenia purpurea*, adsorbed onto the surface of (6,6) armchair CNT using density functional theory (DFT) calculation.

3. Results and Discussion

CNTs or carbon nanotubes describe drug delivery platforms that may be functionalized with various biomolecules containing antibodies, proteins, and DNA. This permits the particular target to transferring the special tissues, organs, or cells. Thus, these compounds can easily penetrate cells, delivering drugs directly to the cytoplasm or nucleus. Drug delivery systems improve the pharmacological and therapeutic profile and efficacy of the drug in question and lower the occurrence of off-target outcomes.

3.1. Nuclear Magnetic Resonance Data

The NMR data of isotropic (σ_{iso}) and anisotropic shielding tensor (σ_{aniso}), as well as the eigenvalues of chemical shielding including σ_{11} , σ_{22} , and σ_{33} (ppm) for (+)-catechin, betulinic acid, ursolic acid, quercetin-3-O-galactoside, luteolin-7-O-glucoside, and myricetin in the *Sarracenia purpurea* medicinal plant, adsorbed onto the surface of (6,6) armchair SWCNT, respectively, have been estimated (Table 1).

Table 1. The results of SCF GIAO magnetic shielding tensor and atomic charge (Q) for (+)-catechin, betulinic acid, ursolic acid, quercetin-3-O-galactoside, luteolin-7-O-glucoside, and myricetin in ppm joint at the adsorption site of (6,6) armchair CNT.

ppm	C9	O10	C16	O17	(+)-catechin C18	O19	H29	H32	H33	
σ_{11}	59.2865	290.7057	83.3679	294.7889	74.8748	314.0021	22.0139	18.3994	22.5452	
σ_{22}	95.0440	290.7057	96.1147	319.9473	102.1597	334.3497	29.1676	30.9900	29.3964	
σ_{33}	202.1101	324.1978	204.8543	371.6628	204.9966	339.3341	40.1023	39.0397	40.7560	
σ_{iso}	118.8135	312.0269	128.1123	328.7997	127.3437	329.2287	30.4279	29.4764	30.8992	
σ_{aniso}	124.9449	18.2563	115.1130	64.2947	116.4793	15.1582	14.5116	14.3450	14.7852	
Q	0.1421	-0.2901	0.116237	-0.2961	0.098471	-0.3090	0.2138	0.2258	0.2213	
ppm	C1	C15	O16	O32	betulinic acid O33	H55	H56	H81		
σ_{11}	-15.6362	169.1082	328.6384	-503.6711	138.8698	28.0314	24.8297	21.7177		
σ_{22}	154.9603	178.9003	337.9158	-252.2589	310.1232	29.9588	31.6255	24.5804		
σ_{33}	164.7082	209.4747	421.9830	450.9700	335.3043	37.4969	49.6449	38.4823		
σ_{iso}	101.3441	185.8277	362.8457	-101.6533	261.4324	31.8290	35.3667	28.2601		
σ_{aniso}	95.0462	35.4704	88.7059	828.9350	110.8078	8.5018	21.4173	15.3332		
Q	0.3171	0.0872	-0.3262	-0.2893	-0.3130	0.0317	0.1843	0.2175		
ppm	C1	C2	O3	O32	ursolic acid O33	H34	H35	H81		
σ_{11}	-14.8985	170.5948	339.4528	-466.2527	149.8814	27.2523	24.1463	22.1181		
σ_{22}	159.4348	178.9689	347.9330	-229.8480	312.0712	28.4278	31.8205	24.5591		
σ_{33}	163.0061	206.2026	420.4447	448.6102	332.2916	39.6026	48.3531	38.8056		
σ_{iso}	102.5141	185.2554	369.2768	-82.4968	264.7481	31.7609	34.7733	28.4942		
σ_{aniso}	90.7380	31.4207	76.7519	796.6605	101.3153	11.7626	20.3697	15.4670		
Q	0.3222	0.0873	-0.3302	-0.2924	-0.3153	0.0342	0.1880	0.2168		
ppm	C9	O10	C16	O17	quercetin-3-O-galactoside C18	O19	H36	H39	H40	
σ_{11}	54.5792	281.0196	76.6664	302.9608	83.8594	322.1996	21.5989	18.9010	22.7514	
σ_{22}	92.8624	322.3705	97.9617	319.2503	118.3675	329.4509	29.5876	30.5873	29.1195	
σ_{33}	201.6165	322.7628	207.5362	372.0312	203.9020	342.7070	38.8885	38.9020	40.9307	
σ_{iso}	116.3527	308.7176	127.3881	331.4141	135.3763	331.4525	30.0250	29.4634	30.9339	
σ_{aniso}	127.8957	21.0677	120.2221	60.9256	135.3763	16.8818	13.2953	14.1579	14.9952	
Q	0.1521	-0.2868	0.1158	-0.2958	0.0999	-0.3038	0.2187	0.2247	0.2208	
ppm	C15	O16	C17	O18	luteolin-7-O-glucoside C23	O24	C25	O26	H38	H39
σ_{11}	80.5725	298.6345	71.3881	308.1253	178.5325	345.1945	175.2961	349.2208	18.1208	22.3625
σ_{22}	99.5240	320.6211	99.9390	331.7684	185.8453	355.1242	183.8870	360.3805	31.1043	29.0165
σ_{33}	203.2873	369.2133	204.0323	340.0012	214.9455	417.7007	210.8215	419.9940	39.1626	40.6486
σ_{iso}	127.7946	329.4896	125.1198	326.6316	193.1078	372.6731	190.0015	376.5317	29.4626	30.6759
σ_{aniso}	113.2391	59.5854	118.3688	20.0544	32.7566	67.5413	31.2300	65.1933	14.5501	14.9591
Q	0.1113	-0.2977	0.1043	-0.3065	0.0689	-0.3163	0.0671	-0.3289	0.2241	0.2229
ppm	C10	O11	C12	C19	myricetin O20	O22	H27	H28	H31	H32
σ_{11}	53.5046	279.3475	99.6682	97.7369	313.5489	316.0992	21.6415	19.8020	18.5542	22.3030
σ_{22}	92.4576	322.1245	142.5628	101.4764	329.1589	334.0617	29.3435	30.2446	31.2943	29.8787
σ_{33}	201.7495	322.9617	223.6607	205.2742	387.8727	337.0559	38.9144	31.4497	39.4524	40.5172
σ_{iso}	115.9039	308.1446	155.2972	134.8292	343.5269	329.0723	29.9665	27.1654	29.7670	30.8996
σ_{aniso}	128.7684	22.2257	102.5452	105.6675	66.5188	11.9754	13.4219	6.4264	14.5282	14.4263
Q	0.1544	-0.2859	-0.1240	0.0836	-0.3111	-0.3086	0.2200	0.0580	0.2343	0.2219

The computed results exhibited the SCF GIAO magnetic shielding tensor in ppm for hydrogen, carbon, and oxygen and explored the active site of (+)-catechin, betulinic acid, ursolic acid, quercetin-3-O-galactoside, luteolin-7-O-glucoside, and myricetin in *Sarracenia purpurea* as the drug for the treatment of the monkeypox disease. The calculations were accomplished based on the B3LYP/6-311+G (2d,p) level of theory using Gaussian 16 revision C.01 program [28] and are reported in Table 1.

The (+)-catechin, betulinic acid, ursolic acid, quercetin-3-O-galactoside, luteolin-7-O-glucoside, and myricetin in *Sarracenia purpurea* medicinal plant, adsorbed onto the (6,6) armchair CNT, showed chemical shielding including σ_{11} , σ_{22} , σ_{33} , σ_{iso} , and σ_{aniso} (ppm) for various atoms of hydrogen, carbon, and oxygen in the active sites of the molecules through the NMR graphs (Figure 1a–f,a'–f'). The most fluctuations of atomic charge and chemical shielding were observed in O10, O19 ((+)-catechin), O16, O32, and O33 (betulinic acid), O3, O32, and O33 (ursolic acid), O10, O17, and O19 (quercetin-3-O-galactoside), O16, O18, O24, and O26 (luteolin-7-O-glucoside) and O11, O20, and O22 (myricetin), respectively (Table 1), due to exploring the most electronegative atoms from those adsorbed onto the surface of (6,6) armchair CNT, which represented the maximal shift in TMS B3LYP/6-311+G(2d,p) (Figure 1a–f).

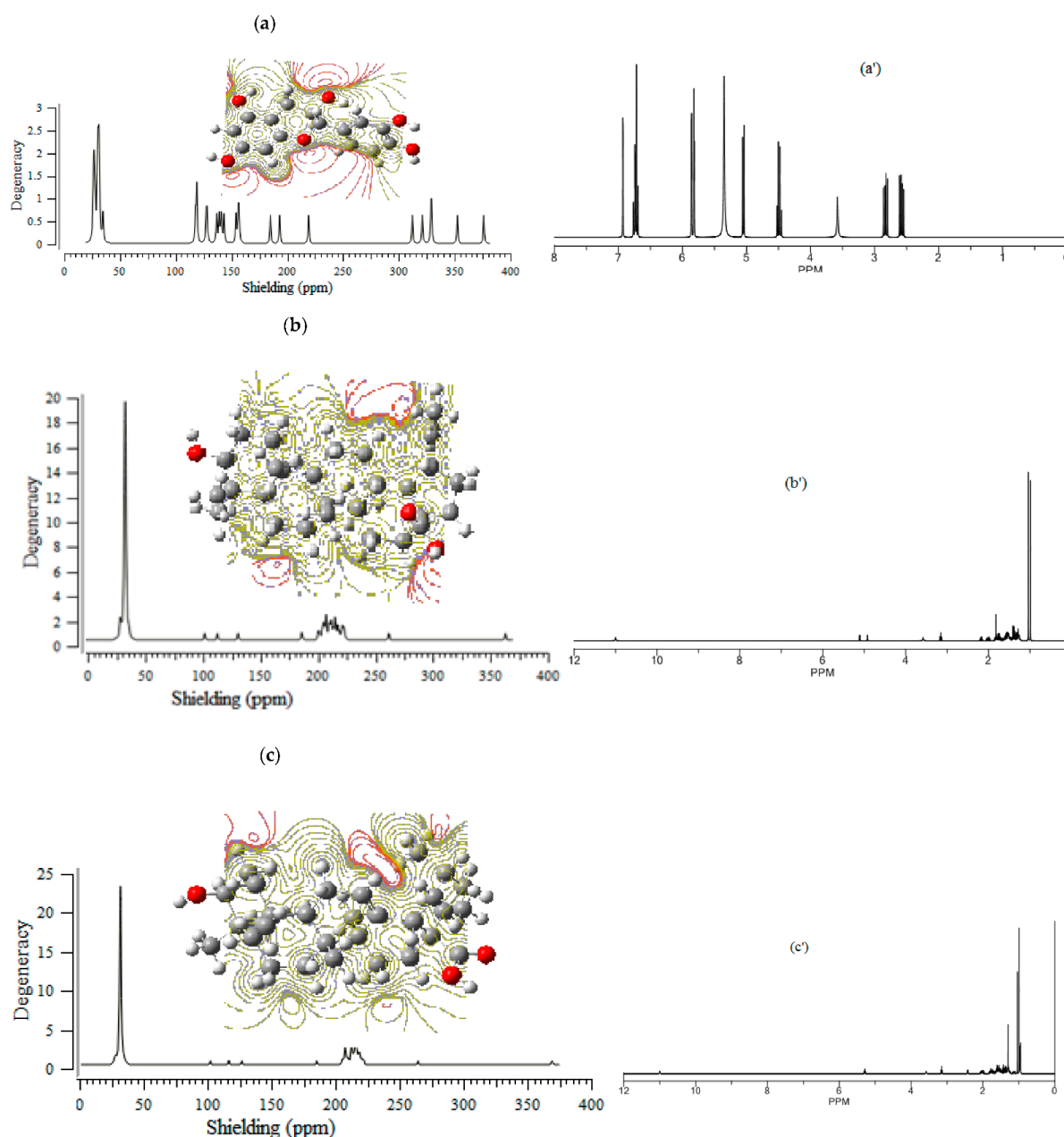


Figure 1. Cont.

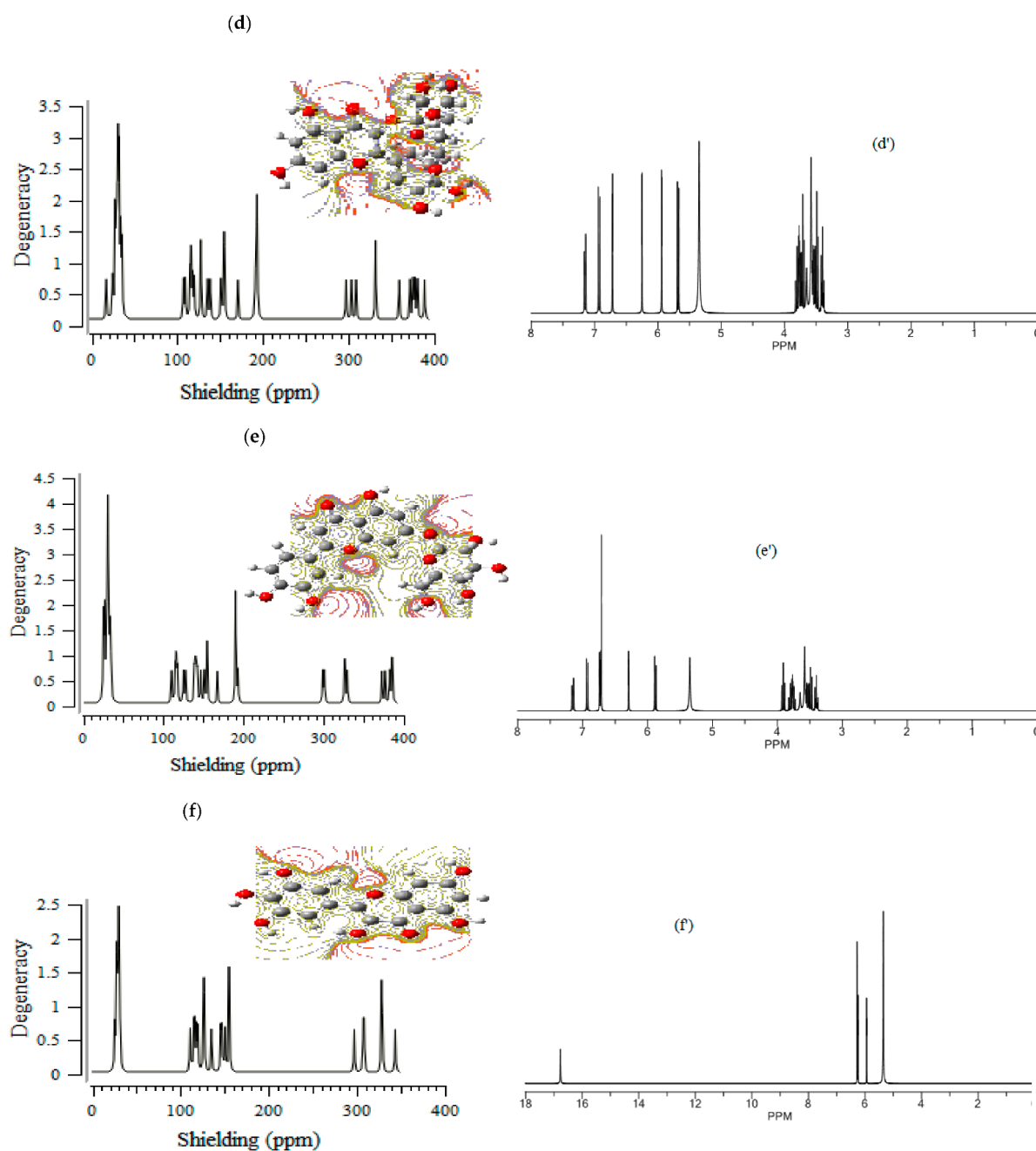


Figure 1. The graph of NMR spectra of isotropic (σ_{iso}), anisotropic (σ_{aniso}) shielding tensors calculated by level of theory B3LYP/6-311+G(2d,p) for (a) (+)-catechin, (a') (+)-catechin→CNT, (b) betulinic acid, (b') betulinic acid→CNT, (c) ursolic acid, (c') ursolic acid→CNT, (d) quercetin-3-O-galactoside, (d') quercetin-3-O-galactoside→CNT, (e) luteolin-7-O-glucoside, (e') luteolin-7-O-glucoside→CNT, (f) myricetin and (f') myricetin→CNT.

CS tensors were yielded by the quantum chemical calculations in the principal axes system to estimate the isotropic chemical shielding (CSI) and anisotropic chemical shielding (CSA) based on the following equations [44–46]:

$$\text{CSI (ppm)} = (\sigma_{33} + \sigma_{22} + \sigma_{11})/3 \quad (1)$$

$$\text{CSA (ppm)} = \sigma_{33} - (\sigma_{22} + \sigma_{11})/2 \quad (2)$$

Additionally, the Onsager model influenced the nuclear magnetic resonance data and chemical shielding of hydrogen, carbon, and oxygen atoms in (+)-catechin, betulinic acid, ursolic acid, quercetin-3-O-galactoside, luteolin-7-O-glucoside, and myricetin, adsorbed onto the surface of (6,6) armchair CNT (Figure 1a–f,a'–f').

Moreover, the electrostatic potential map (ESP) was exhibited, which indicated the region including the attractive–repulsive force of a fix charge at different points in space that were parallel from a molecular surface of (+)-catechin, betulinic acid, ursolic acid, quercetin-3-O-galactoside, luteolin-7-O-glucoside, and myricetin in *Sarracenia purpurea* (Figure 1a–f).

The single-walled (6,6) armchair carbon nanotube was used as an additive to enhance the magnetic and electric sensitivities. These results were attributed to the excellent electromagnetic conductivity of the carbon nanostructure. The recommended mechanism of drug delivery involved (+)-catechin, betulinic acid, ursolic acid, quercetin-3-O-galactoside, luteolin-7-O-glucoside, and myricetin being calculated under the effect of the carbon nanotube and thereby releasing the drug.

3.2. Charge Transfer

Moreover, the results of atomic charge (Q) in Table 1 in a polar medium of water solution indicated the stability of (+)-catechin, betulinic acid, ursolic acid, quercetin-3-O-galactoside, luteolin-7-O-glucoside, and myricetin in *Sarracenia purpurea* drug joint to the surface of (6,6) armchair SWCNT as a drug delivery technique for treating the monkeypox disease (Figure 2).

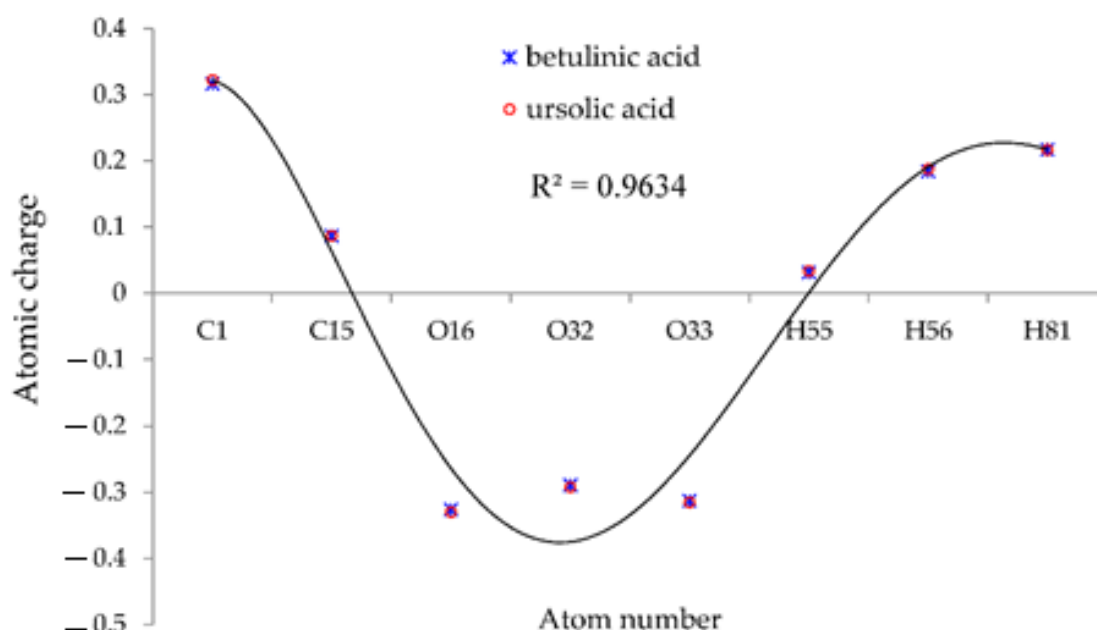


Figure 2. The fluctuation of atomic charge (Q) of hydrogen, carbon and oxygen atoms in the active sites of (+)-catechin, betulinic acid, ursolic acid, quercetin-3-O-galactoside, luteolin-7-O-glucoside, and myricetin.

Figure 2 suggests that the reasons for the various existing observed results of (+)-catechin, betulinic acid, ursolic acid, quercetin-3-O-galactoside, luteolin-7-O-glucoside, and myricetin adsorbed onto the surface of (6,6) armchair SWCNT were principally bound to the position of the active sites of labeled hydrogen, carbon, and oxygen, which move the charge of electrons in these compounds in polar water molecules. In fact, the partial charges were obtained by fitting the electrostatic potential with a correlation coefficient of $R^2 = 0.9634$ to fixed charges of H, C, and O atoms of (+)-catechin, betulinic acid, ursolic acid, quercetin-3-O-galactoside, luteolin-7-O-glucoside, and myricetin, which were adsorbed onto the

surface of (6,6) armchair CNT. Therefore, we assessed the electrophilic side chains of (+)-catechin, betulinic acid, ursolic acid, quercetin-3-O-galactoside, luteolin-7-O-glucoside, and myricetin in *Sarracenia purpurea* medicinal plant to find the reason for the activity and the stability of this drug against monkeypox virus activity.

3.3. Infrared Spectra Analysis

The results of the computational method of the infrared (IR) spectra were accomplished for (+)-catechin, betulinic acid, ursolic acid, quercetin-3-O-galactoside, luteolin-7-O-glucoside, and myricetin, adsorbed onto the surface of (6,6) armchair CNT, by using the B3LYP method and the 6-311+G (2d,p) basis set for atoms including hydrogen, carbon, and oxygen to obtain more accurate equilibrium geometrical parameters, thermodynamic properties and data for each of the determined structures. The IR spectra for (+)-catechin, betulinic acid, ursolic acid, quercetin-3-O-galactoside, luteolin-7-O-glucoside, and myricetin in *Sarracenia purpurea* drug were shown in the frequency range of about 250 cm^{-1} – 4500 cm^{-1} (Figure 3a–f). It can be seen that the strongest allowed peaks with the highest frequency occur around 1425 cm^{-1} , 1650 cm^{-1} , 1700 cm^{-1} , 1725 cm^{-1} , 1900 cm^{-1} , 1925 cm^{-1} , 1950 cm^{-1} , 2100 cm^{-1} , 2150 cm^{-1} ((+)-catechin); 250 cm^{-1} , 650 cm^{-1} , 1400 cm^{-1} , and 2200 cm^{-1} (betulinic acid); 250 cm^{-1} , 1400 cm^{-1} , 1700 cm^{-1} , 2200 cm^{-1} , 3400 cm^{-1} , and 3490 cm^{-1} (ursolic acid); 1300 cm^{-1} , 1550 cm^{-1} , 1700 cm^{-1} , 1950 cm^{-1} , 2150 cm^{-1} , 2200 cm^{-1} , and 3750 cm^{-1} (quercetin-3-O-galactoside); 1350 cm^{-1} , 1800 cm^{-1} , 1950 cm^{-1} , 2150 cm^{-1} , and 2200 cm^{-1} (luteolin-7-O-glucoside), and 1250 cm^{-1} , 1450 cm^{-1} , 1500 cm^{-1} , 1525 cm^{-1} , 1550 cm^{-1} , 1900 cm^{-1} , 1950 cm^{-1} , 2000 cm^{-1} , 2125 cm^{-1} , 2150 cm^{-1} , and 2200 cm^{-1} (myricetin), respectively (Figure 3a–f).

The spectra of Figure 3 demonstrate the reason for the existing observed various results for the frequencies of (+)-catechin, betulinic acid, ursolic acid, quercetin-3-O-galactoside, luteolin-7-O-glucoside, and myricetin, adsorbed onto the surface of (6,6) armchair CNT, which present the position of the active sites of labeled hydrogen, carbon, and oxygen in this drug (Scheme 1). These transfer the charge of electrons in polar (+)-catechin, betulinic acid, ursolic acid, quercetin-3-O-galactoside, luteolin-7-O-glucoside, and myricetin as adsorbates in water toward the surface of (6,6) the armchair carbon nanotube as an adsorbent (Scheme 2).

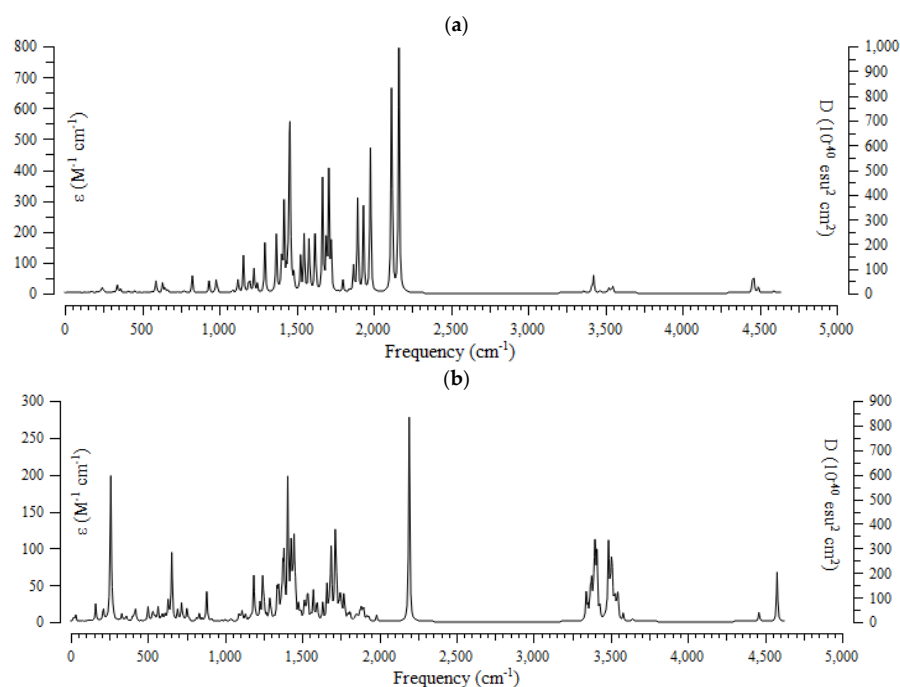


Figure 3. Cont.

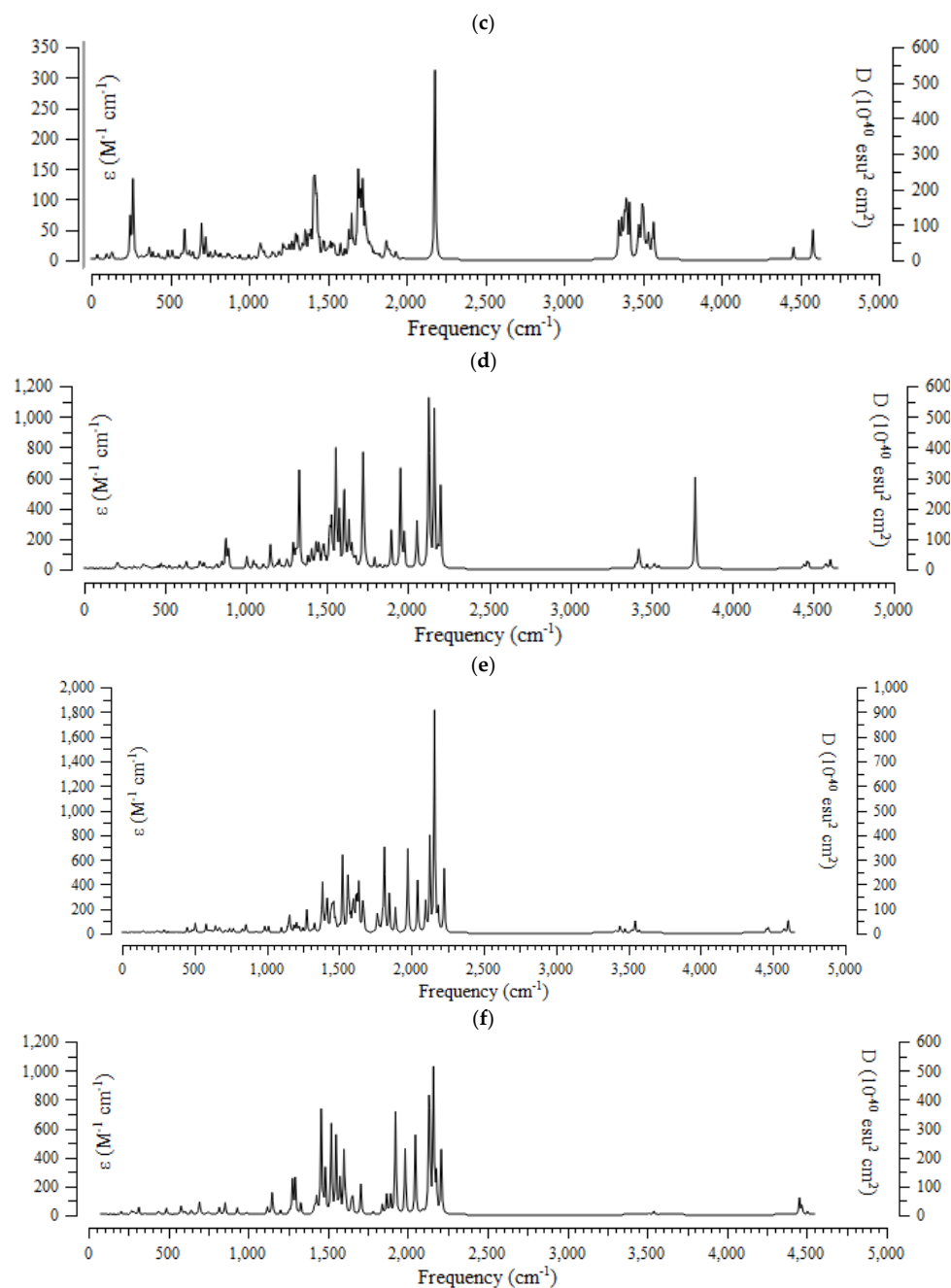


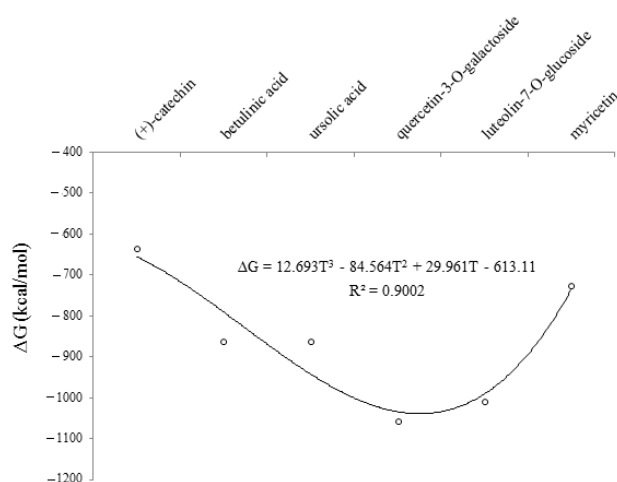
Figure 3. The infrared spectra of effective compounds in *Sarracenia purpurea* drug including (a) (+)-catechin, (b) betulinic acid, (c) ursolic acid, (d) quercetin-3-O-galactoside, (e) luteolin-7-O-glucoside, and (f) myricetin adsorbed onto the surface of (6,6) armchair CNT by using 6-311+G(2d,p) calculations.

The results of physical and thermodynamic properties of dipole moment, ΔH , ΔG and ΔS for (+)-catechin, betulinic acid, ursolic acid, quercetin-3-O-galactoside, luteolin-7-O-glucoside, and myricetin, adsorbed onto the surface of (6,6) armchair CNT using the B3LYP/6-311+G(2d,p) method, are represented in Table 2 and Figure 4.

It was notable that polarization functions into the applied basis set in the computations always demonstrated a significant achievement in the simulation and modeling methods of theoretical levels. The normal modes of IR spectra were explored via harmonic potential wells by analytic methods which kept the movement of all atoms at the same time in the vibration time scale, leading to a natural definition of molecular vibrations (Table 2 and Figure 4).

Table 2. The results of calculated thermodynamic properties of ΔG , ΔH (kcal/mol) and ΔS (cal/mol.K⁻¹) in water at 300 K.

Compounds	$\Delta G \times 10^{-3}$	$\Delta H \times 10^{-3}$	ΔS	Dipole Moment (Debye)
(+)-catechin	-634.993	-634.958	117.270	2.3245
betulinic acid	-860.291	-860.242	161.600	1.5023
ursolic acid	-860.275	-860.229	151.479	1.4017
quercetin-3-O-galactoside	-1055.740	-1055.697	142.287	5.4546
luteolin-7-O-glucoside	-1009.555	-1009.514	138.448	5.4520
myricetin	-726.155	-957.555	112.043	2.2361

**Figure 4.** The changes in Gibbs free energy (ΔG) for (+)-catechin, betulinic acid, ursolic acid, quercetin-3-O-galactoside, luteolin-7-O-glucoside, and myricetin adsorbed onto the surface of (6,6) armchair CNT using B3LYP/6-311+G(2d,p) quantum calculation.

The results of the above observations strongly suggested that (+)-catechin, betulinic acid, ursolic acid, quercetin-3-O-galactoside, luteolin-7-O-glucoside, and myricetin in *Sarracenia purpurea* medicinal plants, adsorbed onto the surface of (6,6) armchair SWCNT using the B3LYP/6-311+G(2d,p) method in a water solvent at 300 K, was predominantly due to basis set functions which were induced by a change in the polarity of the environment. As shown in Figure 4, a curve of degree 3 with the relation coefficient of $R^2 = 0.9002$ proved that an increase in the dielectric constant enhanced the stability and the efficiency of this drug for treating the monkeypox disease.

In fact, single-walled carbon nanotubes reviewed in general physically adsorbed many of the organic molecules considered, and we ameliorated their detecting properties through chemisorption study.

3.4. HOMO and LUMO Analysis

The ionization caused the highest occupied molecular orbital (HOMO) energy and the electron affinity produced the lowest unoccupied molecular orbital (LUMO) energy. These were calculated and their results are reported for (+)-catechin, betulinic acid, ursolic acid, quercetin-3-O-galactoside, luteolin-7-O-glucoside, and myricetin in Table 3. The HOMO, LUMO and band energy gap (eV) presented the pictorial explanation of the frontier molecular orbitals and their respective positive and negative zones, which were important factors for identifying the molecular characteristics of effective compounds in *Sarracenia purpurea* drugs.

Table 3. The HOMO, LUMO and band energy gap (ev) for effective compounds of (+)-catechin, betulinic acid, ursolic acid, quercetin-3-O-galactoside, luteolin-7-O-glucoside, and myricetin in *Sarracenia purpurea* drug.

Compounds	E_{LUMO} (ev)	E_{HOMO} (ev)	$\Delta E = E_{LUMO} - E_{HOMO}$ (ev)
(+)-catechin	-2.1960	-6.7125	4.5165
betulinic acid	-3.5556	-7.6586	4.103
ursolic acid	-3.6444	-7.0303	3.3859
quercetin-3-O-galactoside	-1.0222	-5.4036	4.3814
luteolin-7-O-glucoside	-1.8610	-5.7944	4.7722
myricetin	-1.7644	-5.5318	3.7674

In fact, the HOMO showed the capability to give an electron while the LUMO as an electron acceptor exhibited the capability to achieving an electron. Therefore, the energy gap ($\Delta E = E_{\text{LUMO}} - E_{\text{HOMO}}$) indicated the energy difference between frontier HOMO and LUMO orbital, which introduced stability to the structure and unraveled the chemical activity of the molecule. In this paper, the energy gap established how (+)-catechin, betulinic acid, ursolic acid, quercetin-3-O-galactoside, luteolin-7-O-glucoside, and myricetin interacted with the surface of (6,6) armchair CNT. Besides, frontier molecular orbitals ran an important function in the optical and electrical properties, like in UV-VIS spectra [47].

Figure 5 demonstrates the changes in energy gap ($E_{\text{LUMO}} - E_{\text{HOMO}}$) versus various effective compounds in *Sarracenia purpurea* medicinal plant consisting of (+)-catechin, betulinic acid, ursolic acid, quercetin-3-O-galactoside, luteolin-7-O-glucoside, and myricetin, adsorbed onto the surface of (6,6) armchair CNT using the B3LYP/6-311+G(2d,p) quantum method.

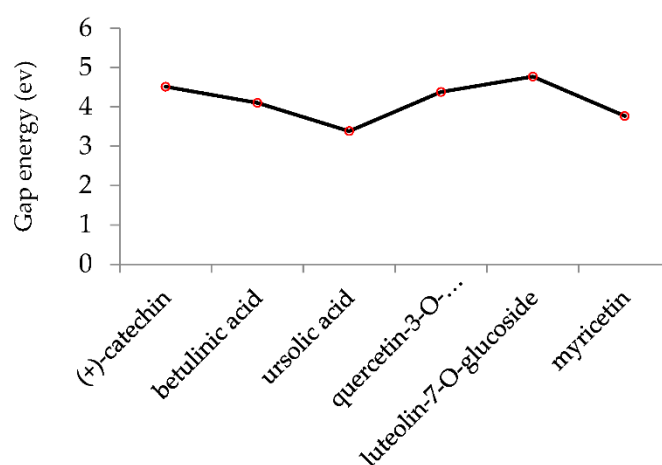


Figure 5. The energy gap (eV) of HOMO–LUMO for (+)-catechin, betulinic acid, ursolic acid, quercetin-3-O-galactoside, luteolin-7-O-glucoside, and myricetin in *Sarracenia purpurea* drug.

Additionally, in order to obtain more conclusive approval in identifying the compound characteristics of these structures, a series of chemical reactivity parameters like chemical potential (μ), electronegativity (χ), hardness (η), softness (ζ), electrophilicity index (ψ) was designed using the following equations (Table 4) [48–50]:

$$\mu = (E_{\text{HOMO}} + E_{\text{LUMO}})/2 \quad (3)$$

$$\chi = -(E_{\text{HOMO}} + E_{\text{LUMO}})/2 \quad (4)$$

$$\eta = (E_{\text{LUMO}} - E_{\text{HOMO}})/2 \quad (5)$$

$$\zeta = 1/(2\eta) \quad (6)$$

$$\psi = \mu^2/(2\eta) \quad (7)$$

The negative amounts of the chemical potential (μ) and the positive values of other quantities exhibited a good stability of (+)-catechin, betulinic acid, ursolic acid, quercetin-3-O-galactoside, luteolin-7-O-glucoside, and myricetin in *Sarracenia purpurea* drug through adsorption onto the surface of (6,6) armchair CNT correlated with the trend of drug delivery (Figure 6). These stable complexes of these compounds with Monkeypox protein virus illustrated the molecular drug delivery.

Table 4. Chemical potential (μ), electronegativity (χ), hardness (η), softness (ζ), electrophilicity index (ψ) for (+)-catechin, betulinic acid, ursolic acid, quercetin-3-O-galactoside, luteolin-7-O-glucoside, and myricetin.

Compound Quantities (ev)	(+)-catechin	Betulinic Acid	Ursolic Acid	quercetin-3-O-galactoside	luteolin-7-O-glucoside	Myricetin
μ	-4.45425	-5.6071	-5.33735	-3.2129	-3.8277	-3.6481
χ	4.45425	5.6071	5.33735	3.2129	3.8277	3.6481
η	2.25825	2.0515	1.69295	2.1907	1.9667	1.8837
ζ	0.2214	0.2437	0.2953	0.2282	0.2542	0.2654
ψ	4.3928	7.6625	8.4135	2.3560	3.7248	3.5326

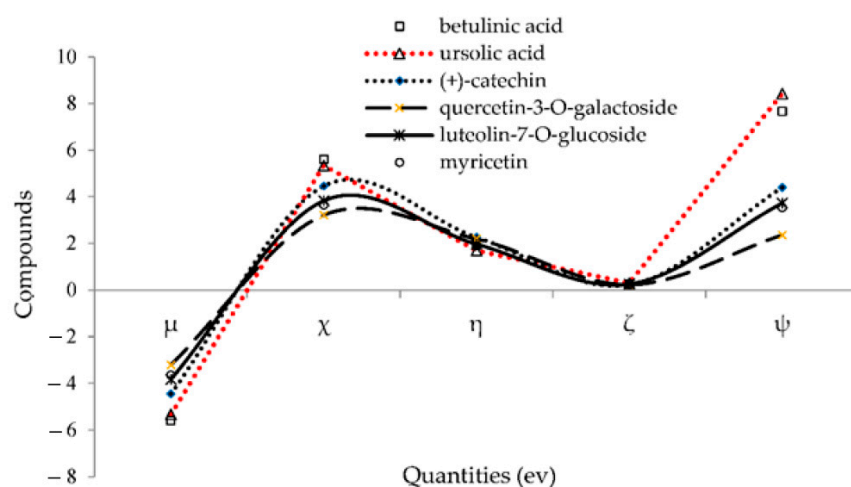


Figure 6. Changes in chemical potential (μ), electronegativity (χ), hardness (η), softness (ζ), electrophilicity index (ψ) for (+)-catechin, betulinic acid, ursolic acid, quercetin-3-O-galactoside, luteolin-7-O-glucoside, and myricetin.

3.5. UV-VIS Spectroscopies

The energy gap between HOMO and LUMO distinguished the attributes of molecular electrical transport [51]. Through the Frank–Condon principle, the maximum absorption peak (max) depended on an ultraviolet–visible (UV-VIS) spectrum to vertical excitation.

In this verdict, TD-DFT/6-311+G (2d,p) computations were performed to identify the low-lying excited states of (+)-catechin, betulinic acid, ursolic acid, quercetin-3-O-galactoside, luteolin-7-O-glucoside, and myricetin in *Sarracenia purpurea* drug. The results consist of the vertical excitation energies, oscillator strength and wavelength introduced in Figure 7a–f.

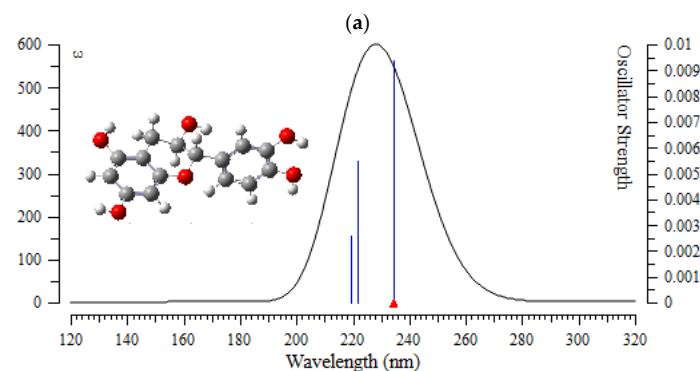


Figure 7. Cont.

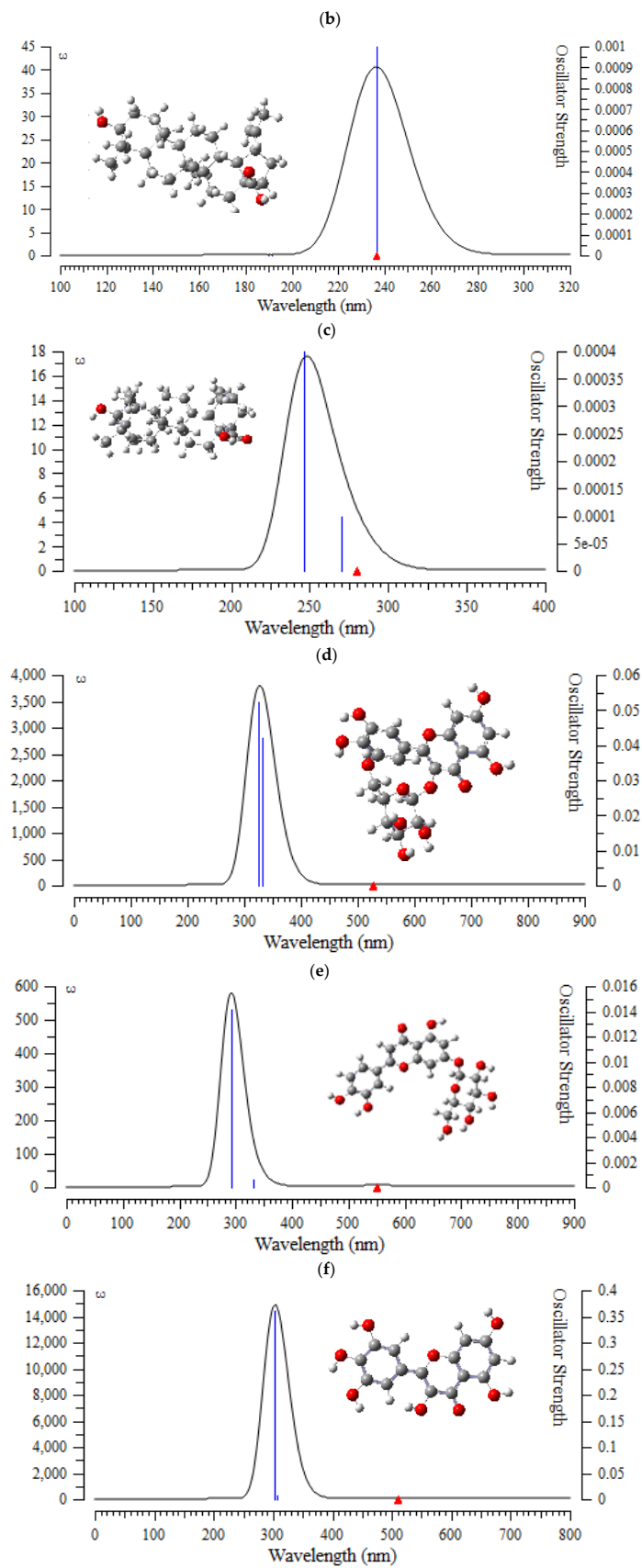


Figure 7. The UV-VIS spectra of (a) (+)-catechin, (b) betulinic acid, (c) ursolic acid, (d) quercetin-3-O-galactoside, (e) luteolin-7-O-glucoside, and (f) myricetin in *Sarracenia purpurea* drug.

In the computed amounts of ultraviolet–visible (UV–VIS) spectra for (+)-catechin, betulinic acid, ursolic acid, quercetin-3-O-galactoside, luteolin-7-O-glucoside, and myricetin extracted from *Sarracenia purpurea* drug, there were maximum adsorption bands between 200 nm–300 nm for (+)-catechin, betulinic acid, ursolic acid with a sharpest peak around 230 nm (Figure 7a–c); and maximum adsorption bands between 200 nm–400 nm for quercetin-3-O-galactoside, luteolin-7-O-glucoside, and myricetin, with the sharpest peak being around 300 nm, respectively (Figure 7d–f). In fact, the intensity of the absorbance of the single-walled (6,6) armchair carbon nanotube was analyzed for (+)-catechin, betulinic acid, ursolic acid, quercetin-3-O-galactoside, luteolin-7-O-glucoside, and myricetin from *Sarracenia purpurea* drug by using ultraviolet–visible (UV–VIS absorption spectroscopy. All nanotubes followed the Lambert–Beer law and indicated similar extinction coefficients irrespective of their structure.

Furthermore, the varieties of theoretical methods were discussed due to comparing density and energies with two approaches of AMBER via Monte Carlo (MC) optimization in water by using a hyperchem professional (7.01) program package. Therefore, the Monte Carlo energies versus time for betulinic acid, (+)-catechin, luteolin-7-O-glucoside, myricetin, quercetin-3-O-galactoside, and ursolic acid, adsorbed onto the surface of (6,6) armchair SWCNT in water medium at 300 K, are plotted in Figure 8.

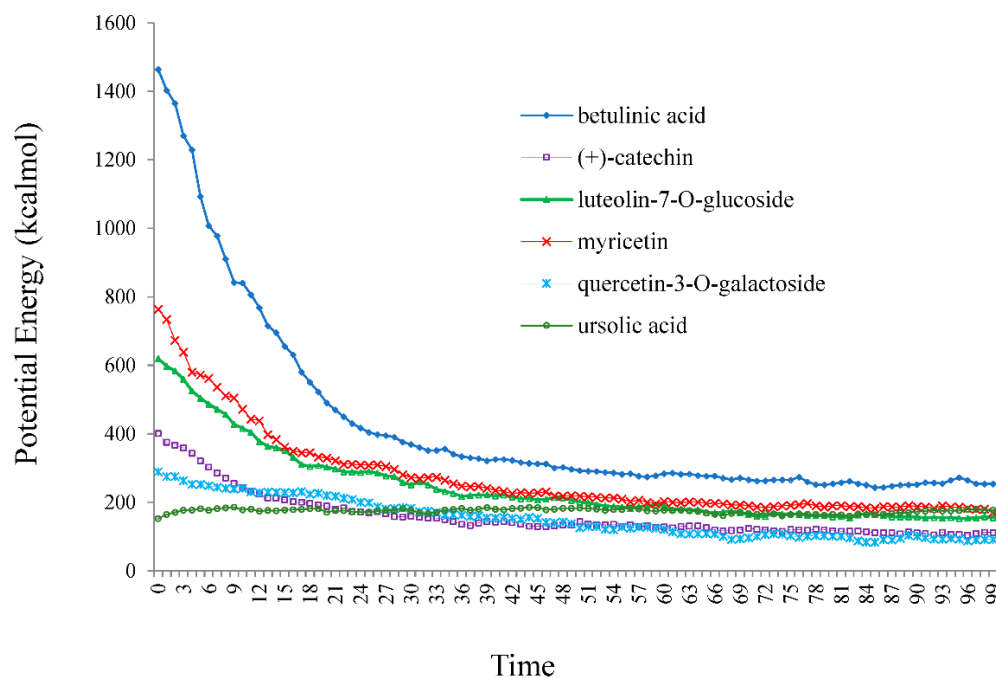


Figure 8. Potential energy (kcal/mol) versus time for betulinic acid, (+)-catechin, luteolin-7-O-glucoside, myricetin, quercetin-3-O-galactoside, and ursolic acid in water at 300 K extracted from Monte Carlo simulation method.

The simulation of betulinic acid, (+)-catechin, luteolin-7-O-glucoside, myricetin, quercetin-3-O-galactoside, and ursolic acid, adsorbed onto the surface of (6,6) armchair SWCNT, showed that the stabilization energy of these compounds was affected by the Monte Carlo force field and temperature in medium of water.

4. Conclusions

Sarracenia purpurea as a medicinal plant can be applied in the prevention the monkey-pox virus through the adsorption of its several effective compounds including (+)-catechin, betulinic acid, ursolic acid, quercetin-3-O-galactoside, luteolin-7-O-glucoside, and myricetin onto the surface of (6,6) armchair single-walled carbon nanotube as the drug delivery model.

This is due to the direct electron transfer principle, which was studied by density functional theory (DFT) methods.

On the other hand, we used the B3LYP/6-311+G (2d,p) level of theory to evaluate the aptitude of SWCNT in adsorbing the effective compounds in *Sarracenia purpurea* medicinal plant through nuclear magnetic resonance and thermodynamic parameters. In fact, the achieved results represented that the feasibility of using (6,6) armchair SWCNT and these compounds became the norm in the drug delivery system which was attained by quantum calculations due to the physico-chemical properties of NMR and IR spectroscopy [52].

Additionally, the energy gap analysis of HOMO–LUMO illustrated the charge distribution in the frontier molecular orbitals of (+)-catechin, betulinic acid, ursolic acid, quercetin-3-O-galactoside, luteolin-7-O-glucoside, and myricetin in *Sarracenia purpurea* drug through adsorption onto the surface of (6,6) armchair carbon nanotube (CNT).

Funding: This research received no external funding.

Data Availability Statement: Not applicable.

Acknowledgments: In successfully completing this paper and its research, the authors are grateful to Kastamonu University for their support through the office, library, and scientific websites.

Conflicts of Interest: The authors declare no conflict of interest.

References

- Petersen, B.W.; Damon, I.K. Smallpox, monkeypox and other poxvirus infections. In *Goldman-Cecil Medicine*, 26th ed.; Lee, G., Andrew, I.S., Eds.; Elsevier: Philadelphia, PA, USA, 2020; Volume 2, pp. 2180–2183. ISBN 978-0-323-53266-2.
- Sutcliffe, C.G.; Rimone, A.W.; Moss, W.J. Poxviruses. In *Hunter's Tropical Medicine and Emerging Infectious Diseases E-Book*, 10th ed.; Ryan, E.T., Hill, D.R., Solomon, T., Aronson, N., Endy, T.P., Eds.; Elsevier: Edinburgh, UK, 2020; pp. 272–277. ISBN 978-0-323-55512-8.
- Harris, E. What to Know About Monkeypox. *JAMA* **2022**, *327*, 2278–2279. [[CrossRef](#)] [[PubMed](#)]
- Simpson, K.; Heymann, D.; Brown, C.S.; Edmunds, W.J.; Elsgaard, J.; Fine, P.; Hochrein, H.; Hoff, N.A.; Green, A.; Ihekweazu, C.; et al. Human monkeypox—After 40 years, an unintended consequence of smallpox eradication. *Vaccine* **2020**, *38*, 5077–5081. [[CrossRef](#)] [[PubMed](#)]
- Bunge, E.M.; Hoet, B.; Chen, L.; Lienert, F.; Weidenthaler, H.; Baer, L.R.; Steffen, R. The changing epidemiology of human monkeypox—A potential threat? *A systematic review. PLoS Negl. Trop. Dis.* **2022**, *16*, e0010141. [[CrossRef](#)]
- Minasov, G.; Inniss, N.L.; Shuvalova, L.; Anderson, W.F.; Satchell, K.J.F. Structure of the Monkeypox virus profilin-like protein A42R reveals potential functional differences from cellular profilins. *Acta Crystallogr. F Struct. Biol. Commun.* **2022**, *78*, 371–377. [[CrossRef](#)]
- Barlow, G.; Irving, W.L.; Moss, P.J. Infectious disease. In *Kumar and Clark's Clinical Medicine*, 10th ed.; Feather, A., Randall, D., Waterhouse, M., Eds.; Elsevier: Amsterdam, The Netherlands, 2020; p. 517. ISBN 978-0-7020-7870-5.
- Hutin, Y.J.; Williams, R.J.; Malfait, P.; Pebody, R.; Loparev, V.N.; Ropp, S.L.; Rodriguez, M.; Knight, J.C.; Tshioko, F.K.; Khan, A.S.; et al. Outbreak of human monkeypox, Democratic Republic of Congo, 1996 to 1997. *Emerg. Infect. Dis.* **2001**, *7*, 434–438. [[CrossRef](#)]
- Arndt, W.; Mitnik, C.; Denzler, K.L.; White, S.; Waters, R.; Jacobs, B.L.; Rochon, Y.; Olson, V.A.; Damon, I.K.; Langland, J.O. In Vitro Characterization of a Nineteenth-Century Therapy for Smallpox. *PLoS ONE* **2012**, *7*, e32610. [[CrossRef](#)]
- Nadar, S.; Khan, T.; Omri, A. Reemergence of monkeypox: Prevention and management. *Expert Rev. Anti-Infect. Ther.* **2022**, *20*, 1425–1433. [[CrossRef](#)]
- Abubakar, I.B.; Kankara, S.S.; Malami, I.; Danjuma, J.B.; Muhammad, Y.Z.; Yahaya, H.; Singh, D.; Usman, U.J.; Ukwuani-Kwaja, A.N.; Muhammad, A.; et al. Traditional medicinal plants used for treating emerging and re-emerging viral diseases in northern Nigeria. *Eur. J. Integr. Med.* **2022**, *49*, 102094. [[CrossRef](#)]
- Millspaugh, C.F. *American Medicinal Plants: An Illustrated and Descriptive Guide to Plants Indigenous to and Naturalized in the United States Which Are Used in Medicine (Illustrated ed.)*; Courier Corporation: Chelmsford, MA, USA, 1892; p. 76. ISBN 9780486230344.
- Mollaamin, F.; Monajjemi, M. Thermodynamic research on the inhibitors of coronavirus through drug delivery method. *J. Chil. Chem. Soc.* **2021**, *66*, 5195–5205. [[CrossRef](#)]
- Tiwari, G.; Tiwari, R.; Sriwastawa, B.; Bhati, L.; Pandey, S.; Pandey, P.; Bannerjee, S.K. Drug delivery systems: An updated review. *Int. J. Pharm. Investig.* **2012**, *2*, 2–11. [[CrossRef](#)]
- Monajjemi, M.; Shahriari, S. Fatemeh Mollaamin, Evaluation of Coronavirus Families & Covid-19 Proteins: Molecular Modeling Study. *Biointerface Res. Appl. Chem.* **2020**, *10*, 6039–6057. [[CrossRef](#)]
- Mollaamin, F. On the behavior of boron nitride Nanotube-Flavin adenine Dinucleotide interaction ion implantation order to design Biofuel cells. *J. Comput. Theor. Nanosci.* **2014**, *11*, 2017–2022. [[CrossRef](#)]

17. Monajjemi, M.; Honaparvar, B.; Khalili Hadad, B.; Ilkhani, A.; Mollaamin, F. Thermo-Chemical Investigation and NBO Analysis of Some anxiolytic as Nano- Drugs. *Afr. J. Pharm. Pharmacol.* **2010**, *4*, 521–529.
18. Singh, A.P.; Biswas, A.; Shukla, A.; Maiti, P. Targeted therapy in chronic diseases using nanomaterial-based drug delivery vehicles. *Signal Transduct. Target. Ther.* **2019**, *4*, 33. [[CrossRef](#)]
19. Mollaamin, F.; Monajjemi, M. Harmonic Linear Combination and Normal Mode Analysis of Semiconductor Nanotubes Vibrations. *J. Comput. Theor. Nanosci* **2015**, *12*, 1030–1039. [[CrossRef](#)]
20. Khaleghian, M.; Zahmatkesh, M.; Mollaamin, F.; Monajjemi, M. Investigation of Solvent Effects on Armchair Single-Walled Carbon Nanotubes: A QM/MD Study. *Fuller. Nanotub. Carbon Nanostructures* **2011**, *19*, 251–261. [[CrossRef](#)]
21. Ghalandari, B.; Monajjemi, M.; Mollaamin, F. Theoretical Investigation of Carbon Nanotube Binding to DNA in View of Drug Delivery. *J. Comput. Theor. Nanosci.* **2011**, *8*, 1212–1219. [[CrossRef](#)]
22. Khalili Hadad, B.; Mollaamin, F.; Monajjemi, M. Biophysical chemistry of macrocycles for drug delivery: A theoretical study. *Russ. Chem. Bull.* **2011**, *60*, 238–241. [[CrossRef](#)]
23. Sarasia, E.M.; Afsharnezhad, S.; Honarparvar, B.; Mollaamin, F.; Monajjemi, M. Theoretical study of solvent effect on NMR shielding tensors of luciferin derivatives. *Phys. Chem. Liquids* **2011**, *49*, 561–571. [[CrossRef](#)]
24. Mollaamin, F. Physicochemical Investigation of Anti-COVID19 Drugs Using Several Medicinal Plants. *J. Chil. Chem. Soc.* **2022**, *67*, 5537–5546. [[CrossRef](#)]
25. Mahdavian, L.; Monajjemi, M. Alcohol sensors based on SWNT as chemical sensors: Monte Carlo and Langevin dynamics simulation. *Microelectron. J.* **2010**, *41*, 142–149. [[CrossRef](#)]
26. Monajjemi, M.; Baheri, H.; Mollaamin, F. A percolation model for carbon nanotube-polymer composites using the Mandelbrot-Given. *J. Struct. Chem.* **2011**, *52*, 54–59. [[CrossRef](#)]
27. Tahan, A.; Mollaamin, F.; Monajjemi, M. Thermochemistry and NBO analysis of peptide bond: Investigation of basis sets and binding energy. *Russ. J. Phys. Chem. A* **2009**, *83*, 587–597. [[CrossRef](#)]
28. Frisch, M.J.; Trucks, G.W.; Schlegel, H.B.; Scuseria, G.E.; Robb, M.A.; Cheeseman, J.R.; Scalmani, G.; Barone, V.; Petersson, G.A.; Nakatsuji, H.; et al. *Gaussian 16, Revision C.01*; Gaussian, Inc.: Wallingford, CT, USA, 2016.
29. Lee, C.; Yang, W.; Parr, R.G. Development of the Colle-Salvetti Correlation-Energy Formula into a Functional of the Electron Density. *Phys. Rev. B* **1988**, *37*, 785–789. [[CrossRef](#)]
30. Koch, W.; Holthausen, M.C. *A Chemist's Guide to Density Functional Theory*, 2nd ed.; Wiley-VCH: Weinheim, Germany, 2000; Volume 3–64, pp. 93–104.
31. Becke, A.D. Density-Functional Exchange-Energy Approximation with Correct Asymptotic Behavior. *Phys. Rev. A* **1988**, *38*, 3098–3100. [[CrossRef](#)]
32. Bakhshi, K.; Mollaamin, F.; Monajjemi, M. Exchange and correlation effect of hydrogen chemisorption on nano V(100) surface: A DFT study by generalized gradient approximation (GGA). *J. Comput. Theor. Nanosci.* **2011**, *8*, 763–768. [[CrossRef](#)]
33. Monajjemi, M.; Khaleghian, M.; Tadayonpour, N.; Mollaamin, F. The effect of different solvents and temperatures on stability of single-walled carbon nanotube: A QM/MD study. *Int. J. Nanosci.* **2010**, *9*, 517–529. [[CrossRef](#)]
34. Cramer, C.J.; Truhlar, D.G. PM3-SM3: A general parameterization for including aqueous solvation effects in the PM3 molecular orbital model. *J. Comp. Chem.* **1992**, *13*, 1089–1097. [[CrossRef](#)]
35. Liotard, D.A.; Hawkins, G.D.; Lynch, G.C.; Cramer, C.J.; Truhlar, D.G. Improved methods for semiempirical solvation models. *J. Comp. Chem.* **1995**, *16*, 422–440. [[CrossRef](#)]
36. Chambers, C.C.; Hawkins, G.D.; Cramer, C.J.; Truhlar, D.G. Model for aqueous solvation based on class IV atomic charges and first solvation shell effects. *J. Phys. Chem.* **1996**, *100*, 16385–16398. [[CrossRef](#)]
37. Giesen, D.J.; Gu, M.Z.; Cramer, C.J.; Truhlar, D.G. A Universal Organic Solvation Model. *J. Org. Chem.* **1996**, *61*, 8720–8721. [[CrossRef](#)] [[PubMed](#)]
38. Onsager, L.J. Electric Moments of Molecules in Liquids. *J. Am. Chem. Soc.* **1936**, *58*, 1486–1493. [[CrossRef](#)]
39. Tomasi, J. Cavity and reaction field: “Robust” concepts. Perspective on “Electric moments of molecules in liquids”. *Theor. Chem. Acc.* **2000**, *103*, 196–199. [[CrossRef](#)]
40. Zadeh, M.A.A.; Lari, H.; Kharghanian, L.; Balali, E.; Khadivi, R.; Yahyaei, H.; Mollaamin, F.; Monajjemi, M. Density functional theory study and anti-cancer properties of shyshaq plant: In view point of nano biotechnology. *J. Comput. Theor. Nanosci.* **2015**, *12*, 4358–4367. [[CrossRef](#)]
41. Mollaamin, F.; Monajjemi, M.; Salemi, S.; Baei, M.T. A Dielectric Effect on Normal Mode Analysis and Symmetry of BNNT Nanotube. *Fuller. Nanotub. Carbon Nanostructures* **2011**, *19*, 182–196. [[CrossRef](#)]
42. Mollaamin, F.; Ilkhani, A.; Sakhaei, N.; Bonsakhteh, B.; Faridchehr, A.; Tohidi, S.; Monajjemi, M.; Fatemeh, M.; Alireza, I.; Neda, S.; et al. Thermodynamic and solvent effect on dynamic structures of nano bilayer-cell membrane: Hydrogen bonding study. *J. Comput. Theor. Nanosci.* **2015**, *12*, 3148–3154. [[CrossRef](#)]
43. Mollaamin, F. Chemotherapy Study of alkaloids through Theoretical Quantum Methods. *Moroc. J. Chemistry.* **2020**, *8*, 400–411. [[CrossRef](#)]
44. Fry, R.A.; Kwon, K.D.; Komarneni, S.; Kubicki, J.D.; Mueller, K.T. Solid-State NMR and Computational Chemistry Study of Mononucleotides Adsorbed to Alumina. *Langmuir* **2006**, *22*, 9281–9286. [[CrossRef](#)]
45. Monajjemi, M.; Noei, M.; Mollaamin, F. Design of fMet-tRNA and Calculation of its Bonding Properties by Quantum Mechanics. *Nucleosides Nucleotides Nucleic Acids* **2010**, *29*, 676–683. [[CrossRef](#)]

46. Monajjemi, M.; Robert, W.J.; Boggs, J.E. NMR contour maps as a new parameter of carboxyl's OH groups in amino acids recognition: A reason of tRNA-amino acid conjugation. *Chem. Phys.* **2014**, *433*, 1–11. [[CrossRef](#)]
47. Aihara, J. Reduced HOMO–LUMO Gap as an Index of Kinetic Stability for Polycyclic Aromatic Hydrocarbons. *J. Phys. Chem. A* **1999**, *103*, 7487–7495. [[CrossRef](#)]
48. Kohn, W.; Becke, A.D.; Parr, R.G. Density Functional Theory of Electronic Structure. *J. Phys. Chem.* **1996**, *100*, 12974–12980. [[CrossRef](#)]
49. Parr, R.G.; Pearson, R.G. Absolute Hardness: Companion Parameter to Absolute Electronegativity. *J. Am. Chem. Soc.* **1983**, *105*, 7512–7516. [[CrossRef](#)]
50. Politzer, P.; Abu-Awwad, F. A comparative analysis of Hartree-Fock and Kohn-Sham orbital energies. *Theor. Chem. Acc.* **1998**, *99*, 83–87. [[CrossRef](#)]
51. Silverstein, R.M.; Bassler, G.C.; Morrill, T.C. *Spectrometric Identification of Organic Compounds*, 5th ed.; John Wiley & Sons, Inc.: New York, NY, USA, 1981.
52. Mollaamin, F. Features of Parametric Point Nuclear Magnetic Resonance of Metals Implantation on Boron Nitride Nanotube by Density Functional Theory/Electron Paramagnetic Resonance. *J. Comput. Theor. Nanosci.* **2014**, *11*, 2393–2398. [[CrossRef](#)]

Disclaimer/Publisher's Note: The statements, opinions and data contained in all publications are solely those of the individual author(s) and contributor(s) and not of MDPI and/or the editor(s). MDPI and/or the editor(s) disclaim responsibility for any injury to people or property resulting from any ideas, methods, instructions or products referred to in the content.